J Solid State Electrochem (2012) 16:403–414
DOI 10.1007/s10008-011-1346-3

ORIGINAL PAPER

Corrosion behavior of AA2024-T3 alloy treated with phosphonate-containing TEOS

Viviane Dalmoro · João H. Z. dos Santos · Denise S. Azambuja

Received: 29 September 2010 / Revised: 1 February 2011 / Accepted: 16 February 2011 / Published online: 6 April 2011

Abstract Protection from corrosion of the aluminum alloy AA2024-T3 coated with a tetraethoxysilicate (TEOS)/aminotrimethyllenephosphonic acid (ATMP) film in a 0.05-mol L^{-1} NaCl solution was evaluated using electrochemical impedance spectroscopy, scanning electron microscopy, energy disperse spectroscopy, and atomic force microscopy. The present work investigates the influence of different pretreatment procedures of the alloy surface and the ATMP concentration on the corrosion resistance of the coated samples. The undoped sol–gel coatings did not provide adequate corrosion protection. The best corrosion protection was achieved using acetic acid pretreatment and subsequent deposition of an ATMP-modified TEOS film with an optimal concentration of 5.00×10^{-4} mol L^{-1} in the deposition bath. The acetic acid pretreatment promotes a decrease in galvanic corrosion and the surface enrichment of aluminum favoring the metalosiloxane and the metal–phosphonic bonds with increasing likely reaction sites, thus promoting the formation of a more homogeneous and compact coating with improved resistance.

Keywords Aluminum alloy · Phosphonate · TEOS · Corrosion

Introduction

AA2024 alloys have been extensively used in many technological applications, such as car manufacturing and the aerospace industry [1]. The presence of copper and magnesium-rich intermetallic particles in these alloys strongly influences the corrosion behavior. The AA2024 alloy is susceptible to pitting corrosion in chloride-containing solutions [2]. To prevent this corrosion, many surface treatments have been proposed, such as silane films which can promote adhesion of the organic coating to metal substrate. Silane films are environmentally friendly treatments, and positive results involving silane films have been obtained with Al and its alloys [3–12], iron and steel [13–17], and Mg and its alloys [18–20].

However, due to the presence of micropores, the coating is affected by low crosslink density moieties, and therefore, the protection efficiency is reduced. One procedure that improves the corrosion properties of the silane layers is doping with corrosion inhibitors [10, 11, 14]. For instance, Quinet et al. [11] reported that sol–gel films doped with an organic redox-active corrosion inhibitor (tetrachloro-*p*-benzoquinone, also named chloranil) are more resistant to corrosion, but the effect is strongly dependent on the concentration of chloranil. Interaction of the inhibitors with the sol–gel layer coating often leads to flaws in the stability of the layer and the activity of the inhibitor. The incorporation of $NaVO_3$ and Na_2MoO_4 into the sol–gel films did not provide suitable corrosion protection due to a decrease in the sol–gel network stability [21].

Maege et al. [22] reported a study of self-assembled monolayers (SAM) on aluminum alloy substrates, including fatty acids, phosphonic or phosphoric acids, alkylsilanes, and alkylsiloxanes. These compounds react spontaneously with Al_2O_3 from the aluminum substrates, leading to a more hydrophobic alloy surface. Of all the studied molecules, the phosphonic acid monolayer gave the best corrosion protection. From an energetic point of view, these molecules consist of three parts: (1) a functional group that is responsible for the

V. Dalmoro · J. H. Z. dos Santos · D. S. Azambuja (✉)
Institute of Chemistry, Federal University of Rio Grande do Sul,
Av. Bento Gonçalves 9500,
CEP 91501-970, Porto Alegre, RS, Brazil
e-mail: denise@iq.ufrgs.br

strong metal–molecule interaction (usually chemisorption), (2) a terminal functional group, which is usually designed according to the application, that determines the characteristics of the modified surface, and (3) a spacer between the functional groups (usually a long alkyl chain) that assures the ordered, close-packed structure of self-assembled layers with a van der Waals interaction between them [23].

The use of organophosphorus coupling molecules in sol–gel processing is very attractive because their reactivity is quite different from that of silicon coupling molecules and leads to different structures and stabilities for the resulting hybrid materials [24].

Khramov et al. [19] studied an anticorrosion surface treatment for magnesium alloy substrates with phosphonate-modified sol–gel-based surface coating processed by a co-reaction of the phosphonate-silane with tetraethoxysilane. Similar results were obtained by Lamaka et al. [20] with phosphonate-functionalized silane. These results were attributed to the formation of hydrolytically stable Mg–O–P chemical bonds.

The incorporation of phenylphosphonic acid in sol–gel films (phenyltrimethoxysilane and tetraethoxysilane) deposited on aluminum was tested as a corrosion inhibitor in a 100-ppm NaCl solution [25]. The more hydrophobic the film, the better the corrosion protection. Films made with tetraethoxysilane provided a minor protection to the Al underneath.

Suitable commercial organosilanes that are effective for corrosion protection are available (e.g., octadecylsilane, 1,2-bis(triethoxysilyl)ethane (BTSE), and bis-[triethoxysilylpropyl]tetrasulfide (BTESPT)), but they are very expensive for routine technological applications. The search for low-cost materials or alternative systems for inhibiting corrosion is demanding. In the present manuscript, we report the effect of the addition of aminotrimethyllenephosphonic acid (ATMP) during the production of a silica-based layer that was produced by the sol reaction of tetraethylorthosilicate (TEOS). Because TEOS contains no organic ligands and forms a film with low hydrophobicity, it was chosen to monitor the effect of the ATMP incorporation.

The corrosion behavior of the AA2024 alloy coated with this resulting system was evaluated using electrochemical impedance spectroscopy (EIS), scanning electron microscopy (SEM), energy disperse spectroscopy (EDS), and atomic force microscopy (AFM). The effect of the nature of the pretreatment alloy and the ATMP initial concentration was investigated.

Experimental

Pretreatments

The surfaces of the AA2024-T3 panels were prepared by grinding with silicon carbide paper up to 1200 grade followed by washing with distilled water and drying under a hot air stream.

The bare alloy samples were submitted to three different pretreatments, which were performed according to the following procedures:

(1) acetic acid pretreatment (ac): immersion in 0.05 mol L^{-1} acetic acid solution for 5 min;
(2) acetic acid–NaOH pretreatment (acnoh): immersion in 0.05 mol L^{-1} acetic acid solution for 5 min followed by immersion in 0.5 mol L^{-1} NaOH for 2 min; and
(3) alkaline pretreatment (noh): immersion in 0.5 mol L^{-1} NaOH for 2 min.

Film deposition

The deposition bath was prepared by mixing tetraethylorthosilicate (TEOS, Merck), ethanol (Nuclear), and distilled water (18.3 MΩ cm^{-2}) in a 4:90:6 (*v*/*v*) ratio. The deposition bath with the inhibitor aminotrimethylenephosphonic acid was prepared by dissolving different amount of ATMP in water corresponding to 6% *v*/*v* in 4% *v*/*v* TEOS and 90% *v*/*v* ethanol. Three concentrations of ATMP were tested in the baths: 5.00×10^{-5}, 5.00×10^{-4}, and 5.00×10^{-3} mol L^{-1}, and the films were denoted as TPA5, TPA4, and TPA3, respectively. The mixture was stirred for 1 h at room temperature and then kept still for up to 3 days prior to use.

After each pretreatment, the samples were washed with distilled water and dried under a hot air stream. Then, the samples were immersed in a sol–gel system for 30 min and cured in an oven at 90 °C for 1 h.

Measurements

A three-electrode electrochemical cell arrangement was used. This apparatus consisted of the AA2024-T3 panel (the working electrode), a Pt wire (counter electrode), and a saturated calomel electrode (SCE; the reference electrode), to which all of the potentials were referred. The electrochemical measurements were performed using an AUTOLAB PGSTAT 30/FRA 2 system. The experiments were carried out at 25 °C. The EIS measurements were performed in potentiostatic mode at the open circuit potential (OCP). The amplitude of the EIS perturbation signal was 10 mV, and the studied frequency ranged from 10^{5} to 10^{-2} Hz. The employed test solution was 0.05 mol L^{-1} NaCl.

SEM and EDS analyses were carried out using a JEOL-JSM 5800 Scanning Microscope with an acceleration voltage of 20 keV. AFM measurements were performed using a Nanoscope IIIa® from Digital Instruments Co. in contact mode using silicon nitride probes.

Results and discussion

The effect of the metal surface pretreatments and the ATMP concentration were evaluated successively by EIS measurements, SEM, and EDS.

Effect of the pretreatments of the AA2024 alloy on the efficiency of deposition of TEOS/ATMP films

The effect of pretreatment was investigated by fixing the concentration of ATMP at 5×10^{-4} mol L^{-1}.

Electrochemical tests

Figure 1 shows the Bode plots of the AA2024 alloy coated with TPA4 that had undergone the three different pretreatments (ac, acnoh, and noh) after 24 and 72 h of immersion in 0.05 mol L^{-1} NaCl.

After 24 h, the sample that had been pretreated with acetic acid (acTPA4) showed a broader phase angle in the 1 kHz−100 mHz frequency range, indicating two overlapped time constants. This result is similar to results

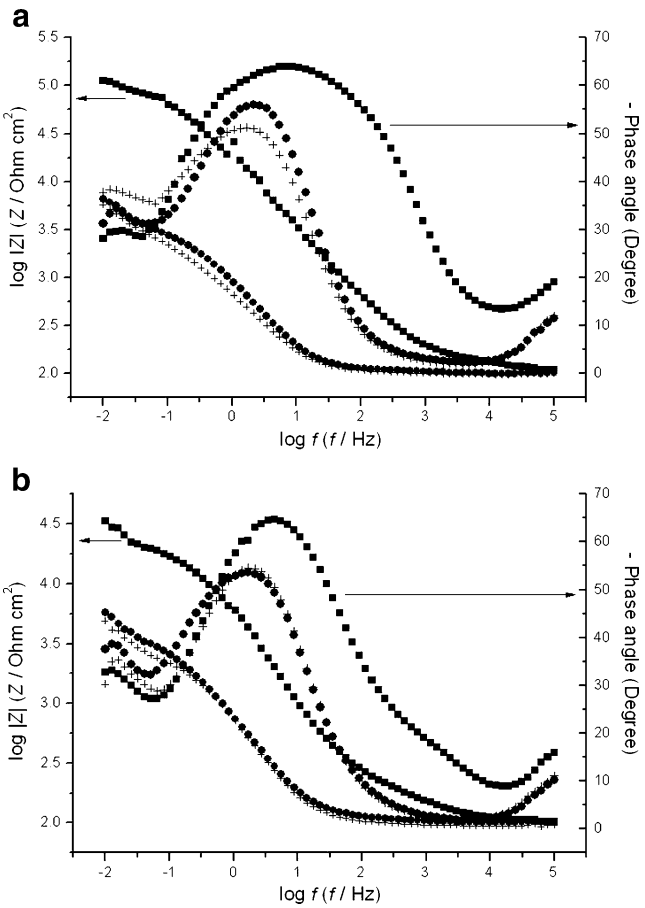

Fig. 1 Bode plots for the AA2024-T3 alloy coated with acTPA4 (*squares*), acnohTPA4(*circles*), and nohTPA4(*plus signs*) films after (**a**) 24 h and (**b**) 72 h immersed in 0.05 mol L^{-1} NaCl

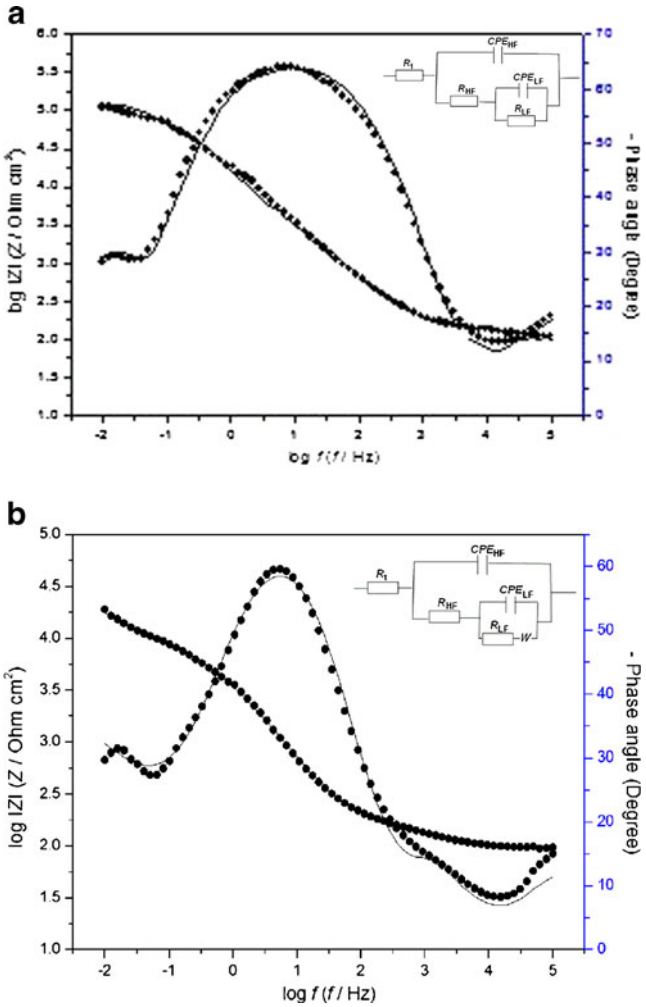

Fig. 2 Experimental and fitted Bode plots for the AA2024-T3 alloy coated with acTPA4 after (**a**) 24 h and (**b**) 7 days immersed in 0.05 mol L^{-1} NaCl

reported in the literature [3, 26]. The coated alloys which were pretreated with NaOH (acnohTPA4 and nohTPA4), a maximum phase angle was detected close to −50° and centered around 2 Hz, indicating the presence of mass transport controlled process [27]. The increased phase angle at higher frequencies for the acTPA4 sample compared to the samples previously pretreated with NaOH suggests that the diffusional contribution decreases with the acTPA4 treatment. For all experimental surface pretreatments after 72 h, the time constants became well defined, and the total impedance modulus ($|Z_t|$) decreased, which may be associated with the occurrence of a corrosion process. However, the sample pretreated with acetic acid showed a $|Z_t|$ value one order of magnitude higher than those observed for the samples with other pretreatments.

The EIS spectra depicted in Fig. 1 for immersion time of 24 and 72 h were fitted using an equivalent circuit (EC) composed of two time constants (insert Fig. 2a), as reported previously in the case of coated samples [3, 11]. The

proposed EC is given by $R_1(CPE_{HF}[R_{HF}(CPE_{LF}R_{LF})])$, where R_1 represents the ohmic resistance between the working and the reference electrodes, CPE_{HF} and R_{HF} represent the capacitance and resistance at the high frequency related to the coating layer, and CPE_{LF} and R_{LF} represent the capacitance and resistance at the low frequency of the interfacial layer that were affected by the presence of pores and defects in the film layer through which the solution can reach the metal surface [28]. According to literature data [7, 9], this interfacial layer consists of an outermost rich Si–O–Si and Si–O–Al layer and an inner Al oxide layer on the alloy substrate. The capacitance was replaced by a constant phase element (*CPE*) that describes a nonideal capacitor when the phase angle is different from −90°. The *CPE* impedance is attributed to the distributed surface reactivity, surface heterogeneity, and roughness of the current and potential distribution, which in turn are related to the electrode geometry and the electrode porosity [29].

For immersion time longer than 90 h, a third time constant represented by a Warburg impedance was included taking into account the diffusion phenomena [26], detected at lower frequencies (Fig. 2b). The proposed EC was used previously for AA2024 coated with silanes [26, 28]. Figure 2a, b shows the experimental and simulated curves obtained for the coated AA2024 alloy pretreated with acetic acid (acTPA4) after 24 h and 7 days of immersion in 0.05 mol L^{-1} NaCl solution. The choice of these EC was carried out with the objective of obtaining a satisfactory fitting of the experimental data, where the circuit elements can be associated with the physical phenomena that are probably taking place on the treated AA2024 electrode surface. The fitting quality was judged based on the error percentage associated to each circuit component, showing errors lower than 5%.

Table 1 presents parameters of the alloy coated with acTPA4 from fitting the experimental impedance spectra after 24 h and 7 days of immersion in 0.05 mol L^{-1} NaCl with the equivalent circuits represented in Fig. 2a, b, respectively.

Figure 3 depicts the evolution of the high and low frequency resistances and capacitances obtained until 72 h of immersion in 0.05 mol L^{-1} NaCl. Increased high frequency resistance (R_{HF}) values were observed after acetic acid treatment. The acTPA4 showed R_{HF} values that are 30 times higher than those observed for the acnohTPA4 and nohTPA4 samples after up to 48 h exposure. After 72 h, the R_{HF} for the acTPA4 and acnohTPA4 were 25.9 and 2.7 kOhm cm^2, respectively. The high frequency capacitance (CPE_{HF}) of the acTPA4 sample increases with time (from 13.3 μF cm^{-2} s^{n-1} after 1 day to 42.8 μF cm^{-2} s^{n-1} after 3 days). These values are five times lower than those observed for the other samples. The R_{HF} describes the coating resistance to electrolyte penetration [3]. Therefore, the observed decreased with the immersion time reflects the coating degradation. The low CPE_{HF} and high R_{HF} for the acTPA4 reveal an

Table 1 Parameters of the silica/phosphonate film/substrate system (acTPA4) obtained from fitting the experimental impedance spectra after 24 h and 7 days of immersion in 0.05 mol L^{-1} NaCl with the equivalent circuits represented in Fig. 2a, b, respectively

	24 h	7 days
R_1 (kOhm cm^2)	115.7	96.8
R_{HF} (kOhm cm^2)	115.3	2.41
CPE_{HF} (μF cm^{-2} s^{n-1})	13.3	87.8
n	0.74	0.83
R_{LF} (kOhm cm^2)	112.3	9.04
CPE_{LF} (mF cm^{-2} s^{n-1})	0.102	0.43
n	0.79	0.80
W (Ohm cm^2 $s^{-1/2}$)	–	3,164.5

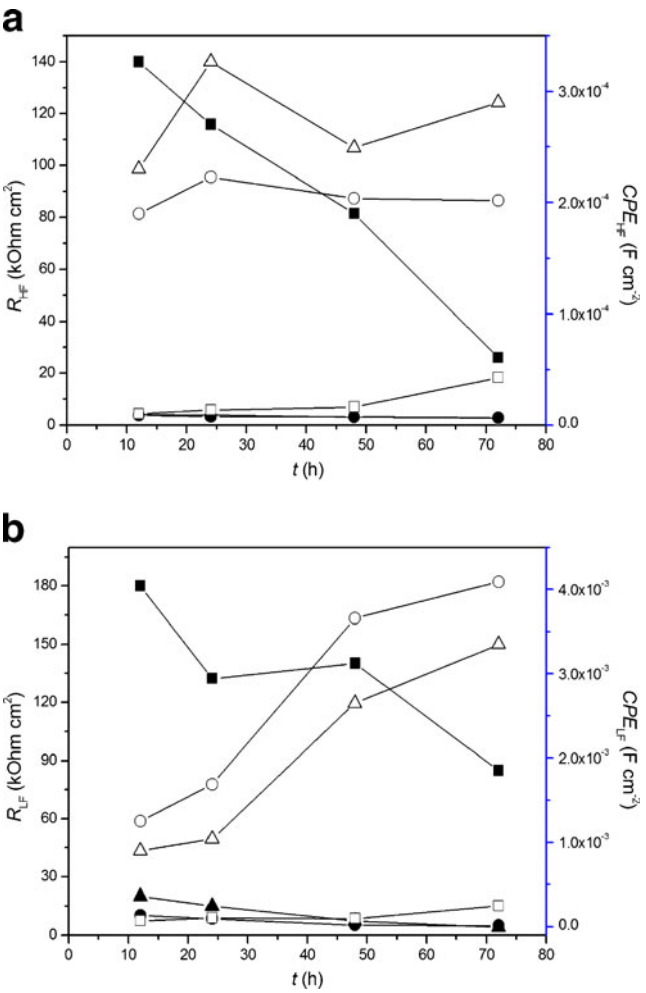

Fig. 3 Evolution of the (**a**) high and (**b**) low frequency capacitances (*open symbols*) and resistances (*full symbols*) of the films acTPA4 (*squares*), acnohTPA4 (*circles*) and nohTPA4 (*triangles*) for different immersion times

improved corrosion protection compared to the acnohTPA4 and nohTPA4.

The low frequency capacitance (CPE_{LF}) increased with exposure for all samples, indicating an enhancement of the corrosion activity of the AA2024-T3 [9]. However, the CPE_{LF} of the acTPA4-treated sample is one order of magnitude lower than that of acnohTPA4 and nohTPA4. The low frequency resistance (R_{LF}) decreases with time. After 72 h, the R_{LF} was equal to 4.9 and 4.1 kOhm cm^2 for the acnohTPA4 and nohTPA4, respectively. For the acTPA4, the R_{LF} was 132.3 kOhm cm^2 after 24 h hand decreased to 84.9 kOhm cm^2 after 72 h. Therefore, the observed decrease with the immersion time reflects the coating degradation.

After 7 days of exposition, the simulated Warburg values were 3,164.5 Ohm cm^2 $s^{-1/2}$, 907.4 Ohm cm^2 $s^{-1/2}$ and 839.2 Ohm cm^2 $s^{-1/2}$ for the coated alloy acTPA4, nohTPA4, and acnohTPA4, respectively. The Warburg element has been related to the diffusion process of the species through the formed porous corrosion products. It was verified that even for longer immersion times in chloride, an increased W value was detected for the alloy pretreated with acetic acid when compared to the other pretreatment. These results confirm that of the three evaluated pretreatments, the acetic acid is the most effective method of retarding the corrosion of AA2024.

Several authors have reported the use of an alkaline treatment prior to silane deposition [5–7]. According to Frignani et al. [5], the immersion of AA7075 alloy in 0.1 mol L^{-1} NaOH for 30 s increases the hydroxyl concentration on the metal surface, promotes the formation of metalo–siloxane bonds, and produces a more protective film. The efficiency of this pretreatment depends on the alloy composition, the exposure time in alkaline solution, and the NaOH concentration. The results obtained in the present work using a solution of 0.5 mol L^{-1} NaOH (pH 12) can be attributed to two factors: the formation of aluminate ions according to the reactions 1 and 2 [30] and the redistribution of copper on the alloy surface [31].

1 $Al + 3OH^- \rightarrow Al(OH)_3 + 3e^-$

2 $Al(OH)_3 + OH^- \rightarrow Al(OH)_4^-$

Copper is highly susceptible to corrosion by acetic acid [32, 33]. Therefore, Cu-rich intermetallic phases present on the AA2024 alloy surface might be preferentially dissolved during the acetic acid pretreatment. SEM images and EDS analysis (not presented here) show a reduction of the amount of Cu on the alloy surface (~20%) after the acetic acid pretreatment compared to an alloy that was only mechanically polished. The superior performance of the ac pretreatment compared to the acnoh and noh pretreatments is mainly due to the decreased galvanic corrosion on the surface alloy because of the lower cathode/anode ratio [34]. Therefore, it is possible to assume that an increase of the surface area of the alloy matrix, as a result of the reduction of Cu amount precipitated on the surface, could take place favoring the metalosiloxane and metal–phosphonic bonds by increasing the number of likely reaction sites.

Microscope examination

Figure 4 shows the SEM and EDS analysis of the uncoated (Fig. 4a) and coated alloy (acTPA4; Fig. 4b) which were pretreated with acetic acid prior to immersion in chloride solution. The presence of irregularities and agglomerates that are randomly distributed on the surface is evidenced, in spite of the substrate preparation by grinding the surface with silicon carbide paper up to grade 1200. The white agglomerates present on bare alloy image were associated to the Al–Cu–Mn–Fe intermetallics according to the EDS analysis (Fig. 4a). These findings are in agreement with those reported in [2, 35]. Two major group particles are observed frequently in AA2024-T3: one is Al_2CuMg (S phase), and the other is Al_6(Cu,Fe, Mn; θ phase). The former is anodic toward the Al matrix, and the latter is cathodic with respect to the Al matrix [36]. The susceptibility to localized corrosion of the AA2024-T3 in chloride solution is deeply related to the difference of electrochemical activity of the intermetallics and that of the matrix [37]. The EDS analysis of the exposed surface of the treated alloy acTPA4 (Fig. 4b) shows a higher silicon amount (around 53%) followed by oxygen (35.4%) and lower concentrations of aluminum (6.3%). The EDS data of the white agglomerates present Al–Cu–Mn–Fe which were associated to the intermetallic particles similar to the bare alloy. The distribution of Si and the other elements varies at different points on the surface of the coated alloy. Hu et al. proposed that the complex composition of the intermetallics in the AA2024 alloy can hinder the formation of a uniform sol–gel film [38], no uniform films being reported by the authors. Hintze and Calle [39] reported that there are a large number of defects on organosilane films deposited on AA2024-T3 when compared to pure aluminum. These defects are probably centered on copper-enriched particles, which are distributed throughout the alloy surface.

The micrographs of the coated samples that underwent the alkaline pretreatment prior to the immersion (Fig. 5a, b) have several irregularities and cracks distributed over the entire surface. These results suggest a highly defective coating. EDS analyses (Fig. 5a, b) of the acnohTPA4 and nohTPA4 samples show high levels of Al followed by Si, Mg, and Cu. The deleterious effect observed with the alkaline treatment is due to an increase in the number of defects and cracks on these coatings. These cracks become preferential zones for the attack of chloride ions. The

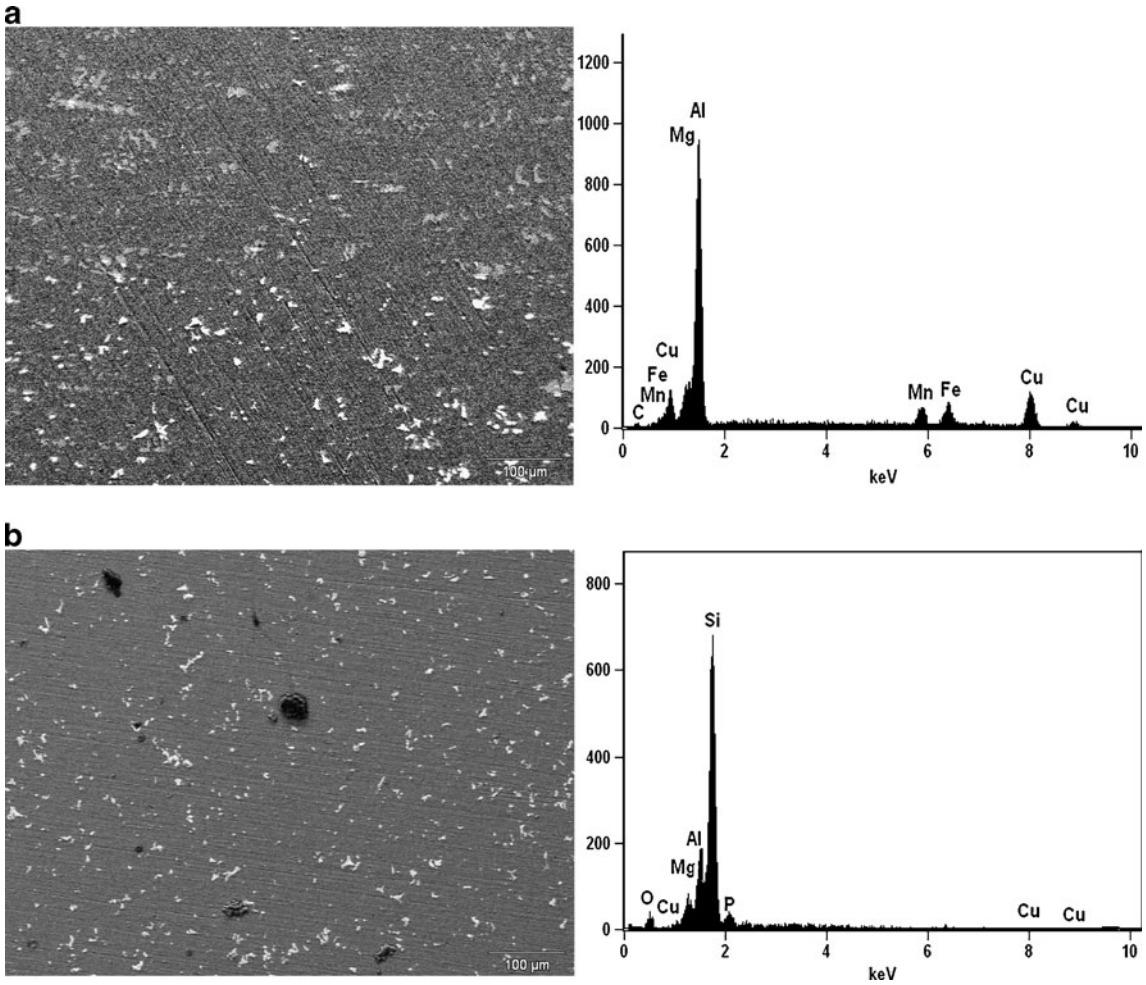

Fig. 4 SEM and EDS analysis of the (**a**) bare alloy AA2024 treated with acetic acid and (**b**) coated with acTPA4 before immersion

presence of similar cracks was detected at galvanized steel covered with γ-mercaptopropyltrimethoxysilane [40], on 3-Glycidoxypropyltrimethoxysilane films on zinc [41], and on hybrid TiO_2/ormosil films on silicon wafers [42].

The SEM images of the coated alloy submitted to the three pretreatments after 48 h of immersion in 0.05 mol L^{-1} NaCl are shown in Fig. 6. For the acTPA4 sample, a higher Si content (close to 43%) and the presence of Al, Cu, and Cl, besides P, which was detected before immersion, are also present after 48 h. The image of nohTPA4 (Fig. 6b) reveals different regions, and the total EDS spectra shows besides the elements Al, Cu, and Mg detected before immersion the presence of Cl. Moreover, this sample becomes swollen due to the electrolyte penetration, and delaminated areas are visible, exposing the bare alloy. The alloy specimen coated with acnohTPA4 after 48 h of immersion shows some agglomerates and cracks (Fig. 6c). Once more, low Si content (8.7%), high Al level (76.8%), and no P were detected. These results are in accordance with the EIS data, where a poor corrosion resistance was obtained with these samples.

Based upon the obtained results, the pretreatment with acetic acid was selected for this work because it exhibits the best performance.

Effect of the ATMP concentration on the corrosion protection of the TEOS/ATMP films

The effect of the ATMP concentration was evaluated by monitoring the corrosion behavior of the alloy that was coated with TEOS after the addition of 5.00×10^{-5}, 5.00×10^{-4}, or 5.00×10^{-3} mol L^{-1} ATMP.

Electrochemical tests

The ATMP addition to TEOS films was tested as a way to obtain a cooperative effect in order to improve the protective characteristics of the coating. The inhibitive efficiency of phosphonic acids is strongly dependent on the concentration [23, 43]. Figure 7 shows the impedance spectra of the bare alloy, the alloy coated with a TEOS film (acTEOS), and the TEOS film with the incorporation of

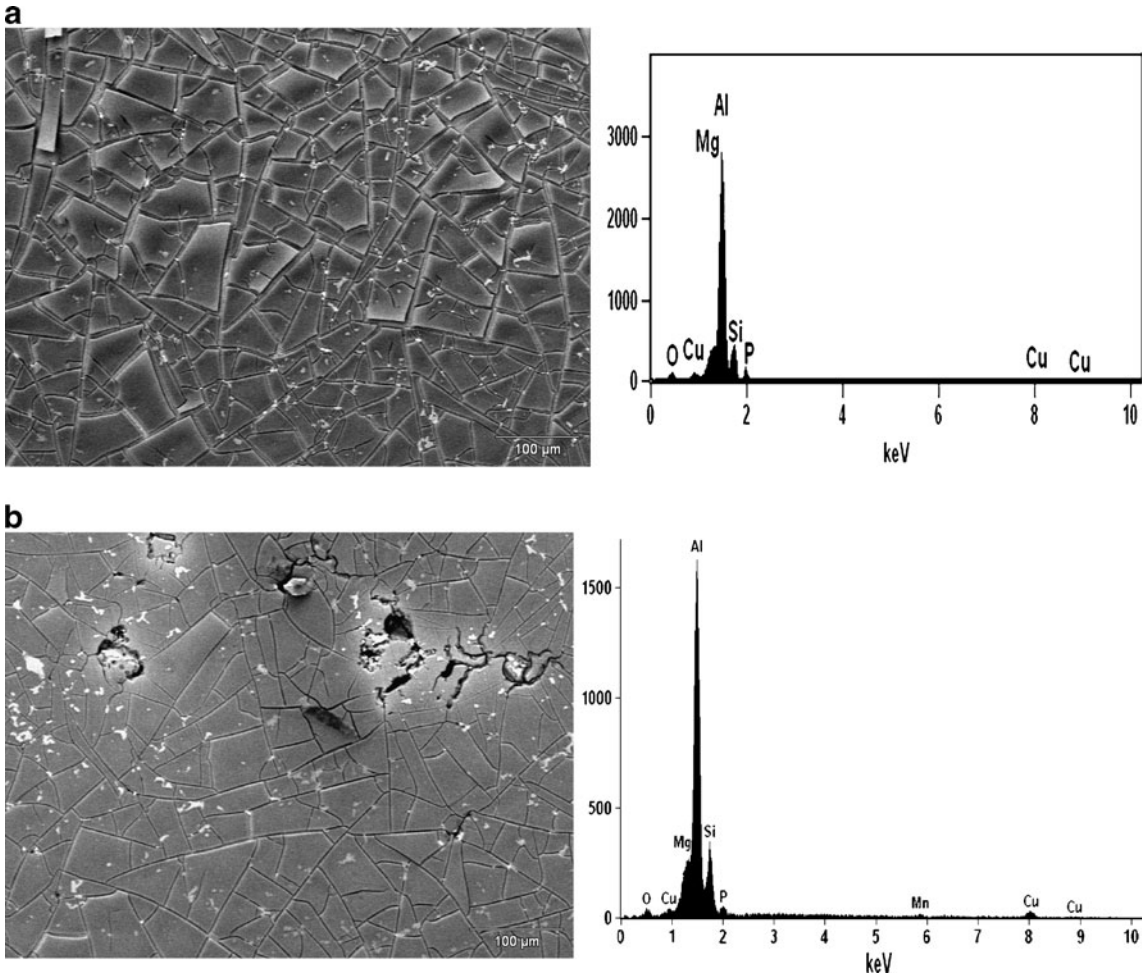

Fig. 5 SEM and EDS analysis for the AA2024 alloy samples coated with (**a**) nohTPA4 and (**b**) acnohTPA4 before immersion

phosphonic acid after 24 and 72 h and 7 days immersed in 0.05 mol L^{-1} NaCl. All of the samples were pretreated with acetic acid.

After 24 h of immersion, the acTPA5 and acTPA3 samples showed similar spectra with two time constants. The process at high frequencies (higher than 2 Hz) is associated with the TEOS/ATMP film on the alloy surface, and the one at lower frequencies corresponds to metal/coating interface phenomena. The overall impedance is increased for the acTPA4, and the lower capacitance values can be explained by a smaller area exposed to the electrolyte attack, possibly due to the inhibiting action of the phosphonic acid impregnated in the TEOS matrix. On increasing the concentration of ATMP to 5.00×10^{-3} mol L^{-1}, a decrease of the total impedance was detected, and a maximum phase angle around −55° at 2 Hz indicates the presence of a film with higher porosity.

The Bode diagram of the alloy coated with a TEOS film (acTEOS) depicts at low frequency (around 100 mHz) inductive points after 24 h. This inductive behavior has been often attributed to Faradaic reactions involving adsorbed intermediate species [44] and also related to active dissolution sites [45] when pitting corrosion propagates [46]. The poor corrosion protection detected with the TEOS film can be attributed to the high hydrophilic character of this coating. The bare alloy spectra after 24-h immersion show two time constants at high and low frequencies with a maximum phase angle around −60° and −40°, respectively. Conde and Damborenea [47] investigated the impedance response of Al–Cu–Mg alloy in NaCl solution being observed a capacitive loop at high frequencies followed by a diffusional behavior corresponding to a Warburg impedance. Thus, according to these authors [47], the high frequency region supplies information of the unattacked surface, while the low frequency impedance can be related to the formation of secondary paths or discontinuities within the Al–oxide layer at or near the incoherent precipitates.

On increasing the immersion time from 72 to 168 h, the EIS spectra of the sample acTPA5, with the lowest concentration of ATMP, showed a decrease of the overall impedance suggesting a degradation of the coating (Fig. 7b, c). The results depict that the sample acTPA4, which

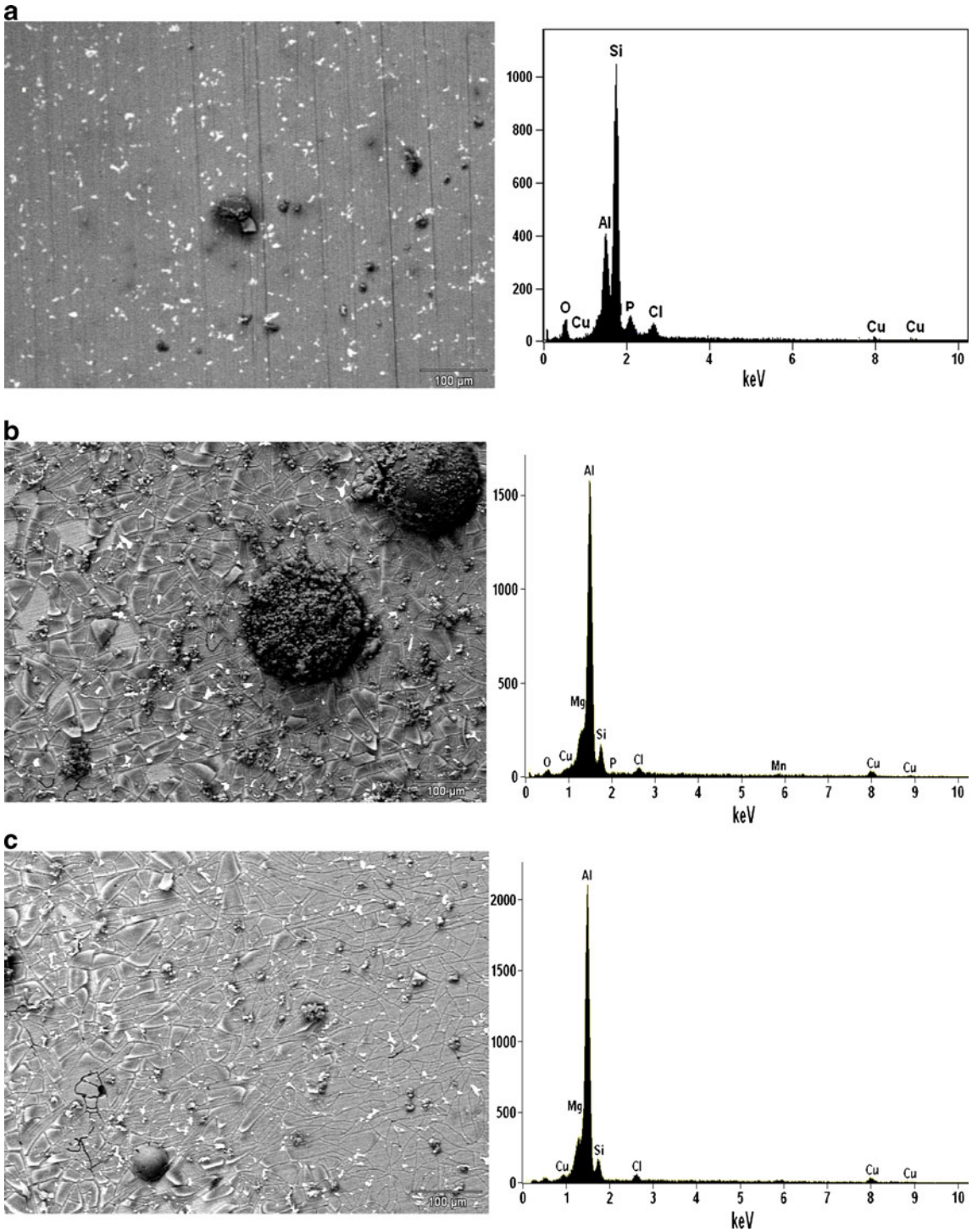

Fig. 6 SEM analysis and EDS spectra for the AA2024 alloy samples coated with (**a**) acTPA4, (**b**) nohTPA4, and (**c**) acnohTPA4 after 48 h of immersion in 0.05 mol L^{-1} NaCl

contains 5.00×10^{-4} mol L^{-1} ATMP, exhibited the best performance in the corrosion test, presenting impedance values almost one order of magnitude higher than those observed for the other coatings (Fig. 7c). These trends suggest that the barrier layer created by the acTPA4-modified TEOS film presented a decreased number of conductive pathways, throughout the electrolyte penetrates reaching the substrate, comparatively to the other coatings. Experimental data obtained after 15 days of immersion (spectra not shown here) evidenced that the corrosion protection caused by the addition of 5.00×10^{-4} mol L^{-1} ATMP to TEOS remains unchanged.

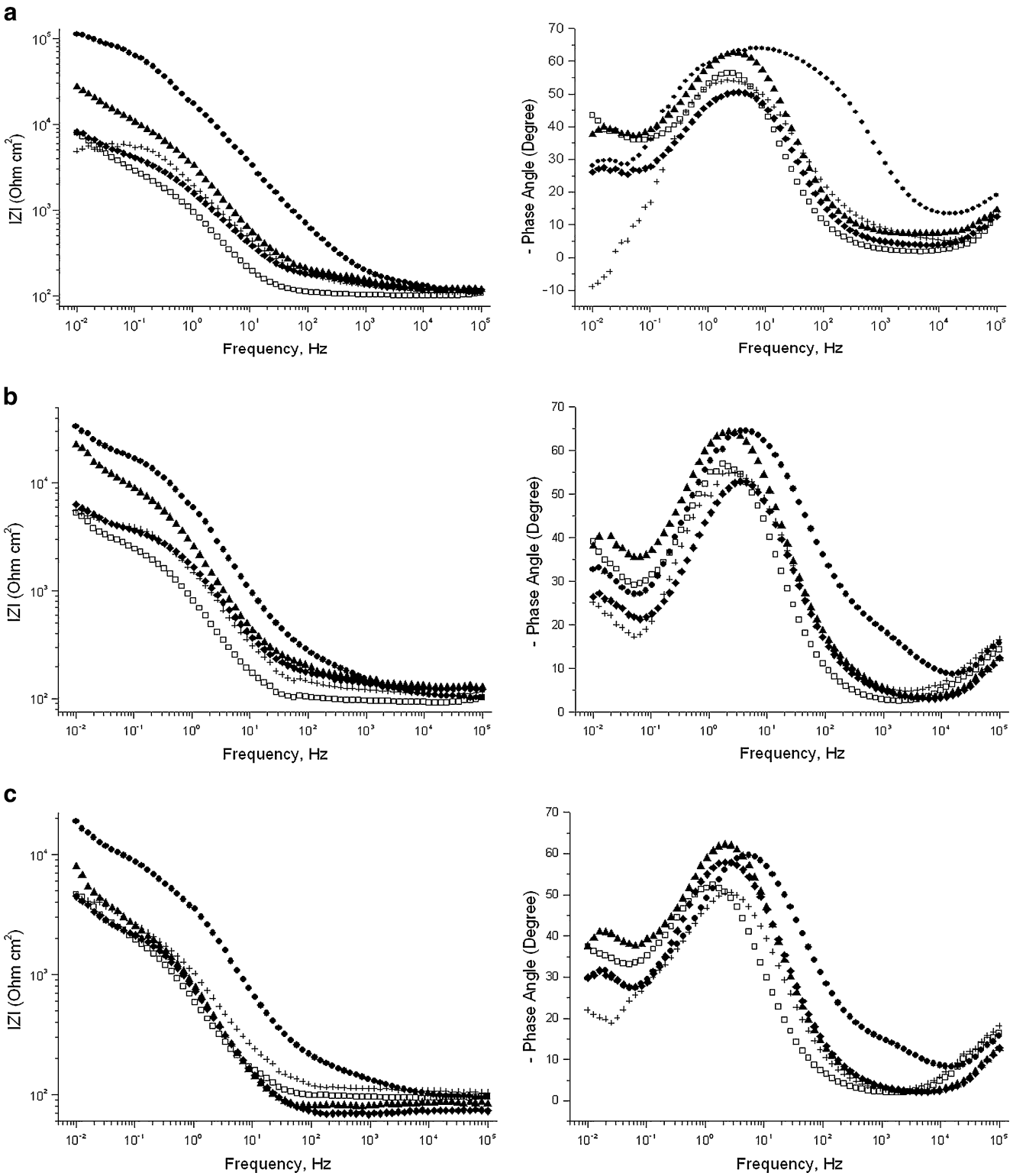

Fig. 7 Bode plots for the AA2024-T3 alloy samples that were uncoated (*squares*) and coated with acTEOS (*plus signs*), acTPA5(*triangles*), acTPA4(*circles*), or acTPA3(*diamonds*) after (**a**) 24 and (**b**) 72 h and (**c**) 7 days immersed in 0.05 mol L^{-1} NaCl

Table 2 Parameters of the silica/phosphonate film/substrate systems with different phosphonate concentration after 48 h of immersion in 0.05 mol L^{-1} NaCl obtained from fitting of the experimental impedance spectra with equivalent circuit given in Fig. 2a

	acTEOS	acTPA5	acTPA4	acTPA3
R_1 (kOhm cm^2)	0.14	0.08	0.10	0.08
R_{HF} (kOhm cm^2)	5.06	6.60	81.4	2.95
CPE_{HF} (μF cm^{-2} s^{n-1})	160.5	154.4	16.2	281.6
n_{HF}	0.75	0.8	0.70	0.80
R_{LF} (kOhm cm^2)	11.9	34.58	140.1	6.79
CPE_{LF} (mF cm^{-2} s^{n-1})	1.90	0.379	0.094	2.57
n_{LF}	0.74	0.78	0.79	0.75

In order to evaluate the effect of ATMP addition on the corrosion resistance of the TEOS-coated AA2024-T3 alloy, the numerical simulation of the experimental data were performed. Table 2 shows the fitting parameters obtained after 48 h of immersion in 0.05 NaCl solution using the EC given in Fig. 2a. From the high frequency parameters, associated with the properties of the film, the resistance for acTPA4 was higher than for the other treated samples. On the other hand, the high frequency capacitance for the acTPA4 sample was lowest, when compared to the other samples. Similar features were detected at the low frequency range.

The film with the addition of 5.00×10^{-4} mol L^{-1} ATMP showed the most improvement to the anticorrosion proprieties of all the TEOS films. More concentrated ATMP solutions have a deleterious effect. Gunasekaran et al. [48] found that high concentrations of phosphonic acid can induce aluminum oxide dissolution when used in solution inhibitors. Therefore, the synergic effect between the aluminum oxide and the silane layer disappears, as already mentioned previously [49]. Felhösi et al. [23] reported that a certain threshold concentration of phosphonate is necessary to ensure sufficient inhibition, being this behavior correlated with surfactant nature of the phosphonic molecules. Moreover, high inhibitor concentration can cause disorganization of the sol–gel network, as reported by Quinet et al. [11].These authors tested the incorporation of tetrachloro-*p*-benzoquinone in a silane matrix. Low concentrations (9.0×10^{-4} mol L^{-1}) produced homogeneous structures with good protective properties of the sol–gel coatings.

Muller and Forster [50] have demonstrated a strong dependence between the Al corrosion inhibition and the phosphonic acid concentration. With increasing concentration of ATMP, the hydrogen evolution increases. Thus, the adequate concentration required to obtain a protective effect must be determined. The authors explained the corrosion inhibition of ATMP based on Pearson's "Principle of Hard and Soft Acids and Bases." Phosphonates (hard Lewis bases) are supposed to form stable complexes with the hard Lewis acid aluminum(III).

AFM analysis

Figure 8 shows the AFM images of the AA2024-T3 bare alloy, the acTEOS sample, and the acTPA4 sample. The image of the bare alloy shows the typical topography of a polished metal. The roughness of the surface is related to the intermetallic particles. According to Schmutz and Frankel [51], these heterogeneities detected at the alloy surface were identified as Al–Cu–(Fe, Mn) and Al–Cu–Mg intermetallic particles, using AFM and XPS techniques. The image of the TEOS coating shows a porous layer with cavities that accompany the roughness of the metal surface. On the other hand, for acTPA4, no lamination marks are observed, indicating that the film covers the entire alloy surface. This feature indicates that the TEOS film that was doped with phosphonic acid is more homogeneous and compact. Based on the present results, it was demonstrated that a cooperative effect can be obtained by using ATMP and TEOS to produce anticorrosive coatings for the AA2024-T3 by selecting an adequate pretreatment of the alloy surface and ATMP concentration.

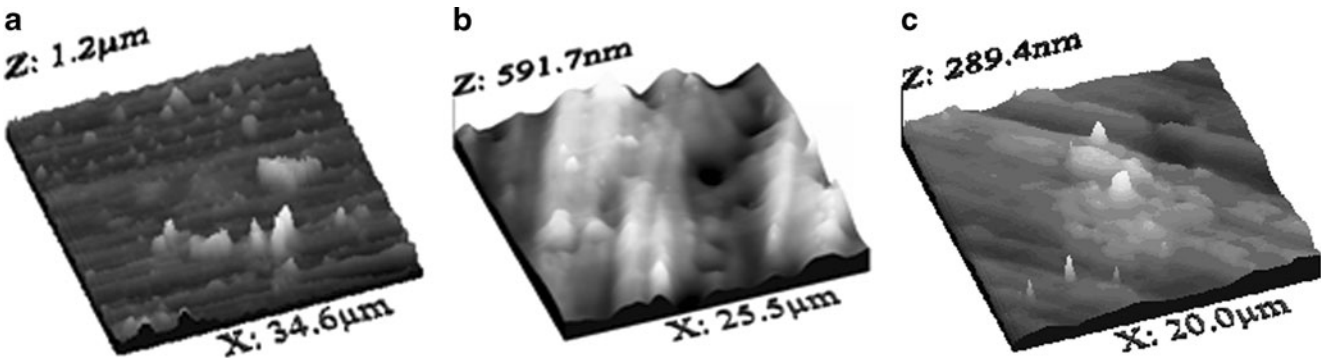

Fig. 8 AFM images of (**a**) bare alloy, (**b**) acTEOS, and (**c**) acTPA4 layer

Conclusion

The corrosion behavior of AA2024-T3 alloy treated with TEOS and phosphonic acid (ATMP) was investigated in 0.05 mol L^{-1} NaCl. The corrosion resistance obtained with films based on TEOS and ATMP was shown to be dependent on the alloy pretreatment and on the phosphonic acid concentration. Among the three pretreatments studied, the acid acetic pretreatment was the most efficient. The superior performance of the ac treatment compared to the acnoh and noh treatments is mainly due to the decreased galvanic corrosion. Therefore, it is possible to assume that the acetic acid pretreatment promotes an increase of the surface area of the alloy matrix, as a result of diminished amount of Cu precipitates on the surface favoring the metalosiloxane and metal–phosphonic bonds, through an increasing of likely reaction sites, keeping a higher resistance along time. The undoped sol–gel coatings did not provide adequate corrosion protection. Coating the AA2024-T3 alloy with TEOS and incorporating an optimal concentration of ATMP (5.00×10^{-4} mol L^{-1} in the deposition bath) decrease the corrosion rate of the metallic substrate, comparatively to the nonmodified TEOS film. This behavior was explained by the strong chemical bonding of phosphonate groups to the aluminum substrate.

Further studies are necessary to understand the interaction of phosphonic acid with the sol–gel network.

Acknowledgments The authors gratefully acknowledge the support of this work by Conselho Nacional de Desenvolvimento Científico e Tecnológico (CNPq).

References

1. Blanc C, Freulon A, Lafont M-C, Kihn Y, Mankowski G (2006) Modelling the corrosion behaviour of Al_2CuMg coarse particles in copper-rich aluminium alloys. Corros Sci 48:3838–3851
2. Buchheit RG, Grant RP, Hlava PF, Mckenzie B, Zender GL (1997) Local dissolution phenomena associated with S phase (Al_2CuMg) particles in aluminum alloy 2024-T3. J Electrochem Soc 144:2621–2628
3. Metroke TL, Gandhi JS, Apblett A (2004) Corrosion resistance properties of Ormosil coatings on 2024-T3 aluminum alloy. Prog Org Coat 50:231–246
4. De Graeve I, Vereecken J, Franquet A, Van Schaftinghen T, Terryn H (2007) Silane coating of metal substrates: complementary use of electrochemical, optical and thermal analysis for the evaluation of film properties. Prog Org Coat 59:224–229
5. Frignani A, Zucchi F, Trabanelli G, Grassi V (2006) Protective action towards aluminium corrosion by silanes with a long aliphatic chain. Corros Sci 48:2258–2273
6. Cabral AM, Duarte RG, Montemor MF, Ferreira MGS (2005) A comparative study on the corrosion resistance of AA2024-T3 substrates pre-treated with different silane solutions: composition of the films formed. Prog Org Coat 54:322–331
7. Cabral A, Duarte RG, Montemor MF, Zheludkevich ML, Ferreira MGS (2005) Analytical characterisation and corrosion behaviour of bis-[triethoxysilylpropyl]tetrasulphide pre-treated AA2024-T3. Corros Sci 47:869–881
8. Wang D, Ni Y, Huo Q, Tallman DE (2005) Self-assembled monolayer and multilayer thin films on aluminum 2024-T3 substrates and their corrosion resistance study. Thin Solid Films 471:177–185
9. Zheludkevich ML, Serra R, Montemor MF, Yasakau KA, Salvado IMM, Ferreira MGS (2005) Nanostructured sol–gel coatings doped with cerium nitrate as pre-treatments for AA2024-T3: corrosion protection performance. Electrochim Acta 51:208–217
10. Moutarlier V, Neveu B, Gidandet MP (2007) Evolution of corrosion protection for sol–gel coatings doped with inorganic inhibitors. Surf Coat Technol 202:2052–2058
11. Quinet M, Neveu B, Moutarlier V, Audebert P, Ricq L (2007) Corrosion protection of sol–gel coatings doped with an organic corrosion inhibitor: chloranil. Prog Org Coat 58:46–53
12. Ji WG, Hu JM, Liu L, Zhang JQ, Cao CN (2007) Improving the corrosion performance of epoxy coatings by chemical modification with silane monomers. Surf Coat Technol 201:4789–4795
13. Wang X, Li G, Li A, Zhang Z (2007) Influence of thermal curing on the fabrication and properties of thin organosilane films coated on low carbon steel substrates. J Mater Process Technol 186:259–264
14. Montemor MF, Trabelsi W, Zheludevich M, Ferreira MGS (2006) Modification of bis-silane solutions with rare-earth cations for improved corrosion protection of galvanized steel substrates. Prog Org Coat 57:67–77
15. Montemor MF, Simões AM, Ferreira MGS, Williams B, Edwards H (2000) The corrosion performance of organosilane based pretreatments for coatings on galvanised steel. Prog Org Coat 38:17–26
16. Flis J, Kanoza M (2006) Electrochemical and surface analytical study of vinyl-triethoxy silane films on iron after exposure to air. Electrochim Acta 51:2338–2345
17. Trabelsi W, Dhouibi L, Triki E, Ferreira MGS, Montemor MF (2005) An electrochemical and analytical assessment on the early corrosion behaviour of galvanised steel pretreated with aminosilanes. Surf Coat Technol 192:284–290
18. Kim J, Wong KC, Wong PC, Kulinich SA, Metson JB, Mitchell KAR (2007) Characterization of AZ91 magnesium alloy and organosilane adsorption on its surface. Appl Surf Sci 253:4197–4207
19. Khramov AN, Balbyshev VN, Kasten LS, Mantz RA (2006) Sol–gel coatings with phosphonate functionalities for surface modification of magnesium alloys. Thin Solid Films 514:174–181
20. Lamaka SV, Montemor MF, Gálio AF, Zheludkevich ML, Trindade C, Dick LF, Ferreira MGS (2008) Novel hybrid sol-gel coatings for corrosion protection of AZ31B. Electrochim Acta 53:4773–4783
21. Voevodin NN, Grebasch NT, Soto WS, Arnold FE, Donley MS (2001) Potentiodynamic evaluation of sol-gel coatings with inorganic inhibitors. Surf Coat Technol 140:24–28
22. Maege I, Jaehne E, Henke A, PAdler H-J, Bram C, Jung C, Stratmann M (1998) Self-assembling adhesion promoters for corrosion resistant metal polymer interfaces. Prog Org Coat 34:1–12
23. Felhösi I, Kálmán E, Póczik P (2002) Corrosion protection by self-assembly. Russ J Electrochem 38:230–237, From (2002) Elektrokhimiya 38:265–273
24. Mutin PH, Guerrero G, Vioux A (2005) Hybrid materials from organophosphorus coupling molecules. J Mater Chem 15:3761–3768
25. Sheffer M, Groysman A, Starosvetsky D, Savchenko N, Mandler D (2004) Anion embedded sol–gel films on Al for corrosion protection. Corros Sci 46:2975–2985
26. Palomino LEM, Suegama P, Aoki IV, Pászti Z, Melo HG (2007) Investigation of the corrosion behaviour of a bilayer cerium-silane pre-treatment on Al 2024-T3 in 0.1 M NaCl. Electrochim Acta 52:7496–7505

27. Walter GW (1986) A review of impedance plot methods used for corrosion performance analysis of painted metals. Corros Sci 26:681–703
28. Tamborim SM, Maisonnave APZ, Azambuja DS, Englert GE (2008) An electrochemical and superficial assessment of the corrosion behavior of AA 2024-T3 treated with metacryloxypropylmethoxysilane and cerium nitrate. Surf Coat Technol 202:5991–6001
29. Jorcin J-B, Orazen ME, Pébère N, Tribollet B (2006) CPE analysis by local electrochemical impedance spectroscopy. Electrochim Acta 51:1473–1479
30. Pourbaix M (1963) Atlas d´equilibres electrochimiques. Gauthier-Villars & Cie Éditeur-Imprimeur-Libraire, Paris, p 168
31. Williams G, Coleman AJ, McMurray HN (2010) Inhibition of aluminium alloy AA2024-T3 pitting corrosion by copper complexing compounds. Electrochim Acta 55:5947–5958
32. Bastidas DM, La Iglesia VM (2007) Organic acid vapours and their effect on corrosion of copper: a review. Corros Eng Sci Tech 42:272–280
33. Gil H, Leygraf C (2007) Quantitative in situ analysis of initial atmospheric corrosion of copper induced by acetic acid. J Electrochem Soc 154:C272–C278
34. Palomino LEM, Castro JFW, Aoki IV, Melo HG (2003) Microstructural and electrochemical characterization of environmentally friendly conversion layers on aluminium alloys. J Braz Chem Soc 14:651–659
35. Liao C-M, Olive JM, Gao M, Wei RP (1998) In-situ monitoring of pitting corrosion in aluminum alloy 2024. Corros Sci 54:451–458
36. Zhu D, van Ooij WJ (2003) Corrosion of AA 2024-T3 by bis-[3-(triethoxysilyl)propyl]tetrasulfide in neutral sodium chloride solution. Part 1: corrosion of AA2024-T3. Corros Sci 45:2163–2175
37. Suter T, Alkire RC (2001) Microelectrochemical studies of pit iniation at single inclusions in Al 2024-T3. J Electrochem Soc 148:B36–B42
38. Hu J-H, Liu L, Zhang J-Q, Nao C-N (2006) Effects of electrodeposition potential on the corrosion properties of bis-1, 2-[triethoxysilyl] ethane films on aluminum alloy. Electrochim Acta 51:3944–3949
39. Hintze PE, Calle LM (2006) Electrochemical properties and corrosion protection of organosilane self-assembled monolayers on aluminum 2024-T3. Electrochim Acta 51:1761–1766
40. Bexell U, Grehk TM (2007) A corrosion study of hot-dip galvanized steel sheet pre-treated with γ-mercaptopropyltrimethoxysilane. Surf Coat Technol 201:4734–4742
41. D-j F, X-h M, Y-m Z, Z-l C, Liu M, F-x G (2009) Preparation of non-chromium polymer films on zinc for corrosion protection due to a compound effect between silane and cerium salt. Anti-Corros Methods Mater 56:226–231
42. Wang B, Hu L (2006) Optical and surface properties of hybrid TiO_2/ormosil planar waveguide prepared by the sol–gel process. Ceram Int 32:7–12
43. To XH, Pébère N, Pelaprat N, Boutevin B, Hervaud Y (1997) A corrosion-protective film formed on carbon steel by an organic phosphonate. Corros Sci 39:295–303
44. Orazen ME, Tribollet B (2008) Electrochemical impedance spectroscopy. Wiley, New Jersey, pp 163–181
45. Brett CM (1990) The application of electrochemical impedance techniques to aluminium corrosion in acidic chloride solution. J Appl Electrochem 20:1000–1003
46. Bessone J, Mayer C, Juttner K, Lorenz WJ (1983) AC-impedance measurements on aluminium barrier type oxide films. Electrochim Acta 28:171–175
47. Conde A, Damborenea J (1997) An electrochemical impedance study of a natural aged Al-Cu-Mg alloy in NaCl. Corros Sci 39:1925–1934
48. Gunasekaran G, Palanisamy N, Appa Rao BV, Muralidharan VS (1997) Synergistic inhibition in low chloride media. Electrochim Acta 42:1427–1434
49. Beccaria AM, Chiaruttini L (1999) The inhibitive action of metacryloxypropylmethoxysilane (MAOS) on aluminium corrosion in NaCl solutions. Corros Sci 41:885–889
50. Muller B, Förster I (1996) Derivatives of phosphoric and phosphonic acid as corrosion inhibitors for zinc pigments. Corros Sci 38:1103–1108
51. Schmutz P, Frankel GS (1998) Corrosion study of AA2024-T3 by scanning Kelvin probe force microscopy and in situ atomic force microscopy stretching. J Electrochem Soc 145:2295–2306